Time-resolved velocity profile measurement using event-based imaging

C. E. Willert[1]*, J. Klinner[1]

[1] German Aerospace Center (DLR), Institute of Propulsion Technology, 51170 Köln, Germany

* chris.willert@dlr.de

Abstract

We describe the implementation of time-resolved velocity profile measurement using event-based vision (EBV) employing an event-camera in-place of a high-speed camera. A narrow light sheet provided by a pulsed laser is imaged by a narrow region of interest on the event camera sensor which allows the capture of a dense particle field. Subsequent multi-frame processing is employed in an off-line manner to retrieve time-resolved velocity profiles from which statistics and spectra can be obtained. The described system is capable of providing data quality on par with currently used, considerably more expensive, high-speed PIV hardware at equivalent frame rate of 10 kHz. The technique is demonstrated with measurements of a fully developed turbulent boundary layer in a wind tunnel at free-stream speeds up to 10 m/s. The data is directly compared to high-speed profile-PIV measurements obtained on the same facility at matching operating and regions of interest.

1 Introduction

1.1 Event-based imaging and its application in particle imaging

Event-based vision (EBV), dynamic vision sensing (DVS) or neuromorphic imaging describe a rather new sub-field within computer vision, differing considerably from classical frame-based imaging (Gallego et al., 2022). Rather than providing rectangular arrays of exposed sensor pixels, i.e. images, event-cameras provide an asynchronous stream of *events* consisting of pixel coordinates, time stamp and a binary contrast change signal. In this sense, event cameras only record contrast changes on the pixel level, either going from dark to bright (positive event) or bright-to-dark (negative event). Static areas in the scene provide no information. In the context of particle imaging, narrow event streaks are produced in the 2d-space-time domain and can be processed to provide 3D-3C particle tracking velocimetry (PTV) data in either real-time (Rusch and Rösgen, 2021, 2022) or offline (Borer et al., 2017; Drazen et al., 2011; Howell et al., 2020). The recently introduced event-based imaging velocimetry (EBIV) technique combines EBV and light sheet illumination to provide time-resolved, planar (2D-2C) velocity fields (Willert and Klinner, 2022; Willert, 2023)).

The profile-PIV technique as introduced by Willert (2015) has been extensively used to obtain both detailed velocity statistics as well as time-resolved data of turbulent flows in a variety of applications Cuvier et al. (2017); Willert et al. (2017, 2018, 2021). The technique relies on imaging a narrow field of view, typically in the wall-normal direction, which allows high-speed cameras to operate at considerably higher framing rates (> 10 kHz) as when operated at full resolution. The field of view is generally illuminated by a high-speed pulsed laser that is collimated into a narrow light sheet (Fig. 1). Seeding is equivalent to the 1 μm aerosol seeding used for conventional PIV is air.

In the folllowing, we introduce the use of event-based imaging to obtain profiles of turbulent quantities in analogy to the profile-PIV technique, hereafter referred to as *event-based profile imaging velocimetry* or just *profile-EBIV*.

2 Measurements

2.1 Test facility and reference measurements

Measurements of a fully developed turbulent boundary layer (TBL) are performed in the 1 m windtunnel of DLR Institute of Aerodynamics and Flow Technology in Göttingen at free stream velocities of $U_\infty = 5 - 20$ m/s. The section has a width $W = 1000$ mm and height $H = 800$ mm. The TBL is tripped at the end of the contraction nozzle by a 10 mm wide zig-zag tape of 750 μm thickness with 10 mm period and 4 mm serrations. The measurement position is located on the tunnel centerline at $x = 2110$ mm downstream of the tripping point. At this point the TBL has a thickness $\delta_{99} \approx 40$ mm. With an aspect ratio of $W/\delta_{99} = 25$, effects due to the tunnel side walls can be assumed to minimal in comparison to many other TBL measurements reported in the literature.
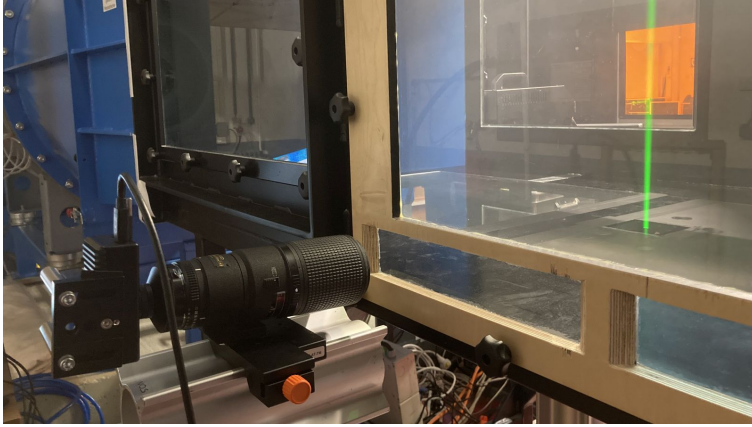

Figure 1: Imaging setup for velocity profile measurements in the 1m wind tunnel of DLR Göttingen. The narrow light sheet has a width of about 5 mm and thickness of about 200 μm and is produced by a pulsed laser of 10 W integral power. An event camera (Prophesee EVK2-HD, 1280×720) with a 200 mm macro-lens records the illuminated particles with reduced field of view.

Reference measurements are obtained using the profile-PIV technique (Willert, 2015). Illumination is provided by a high-speed pulsed laser with maximum integral power of 10 W at a wavelength $\lambda = 532$ nm (NanioAir, Innolas Photonics). A light sheet of about 10 mm width and ≈ 300 μm waist thickness is introduced through a thin glass window on the centerline of the test section's bottom wall (cf. Fig. 1). The tunnel is (densely) seeded with water/glycol based aerosol seeding from a vaporizer fog generator (HazeBase Classic). The illuminated tracers are imaged by a high-speed camera (V2640, Vision Research, 2048×1952 pixel, 144GB) fitted with a $f = 200$ mm macro lens (Nikon Micro-Nikkor 200/4). The image magnification is set to $1.25\times$ the vertical extent of the boundary layer to properly characterize the TBL. At this magnification the high-speed camera resolves the viscous scale $l^+ = \nu/u_\tau$ with 2.6 pixel at the lower speed of $U_\infty = 5.2$ m/s, reducing to 1.5 pixel at $U_\infty = 10.0$ m/s.

For the high-speed profile-PIV measurements the laser pulse rate is adjusted to maintain a similar particle image displacement (20 pixel) for the three different tunnel velocities (see Table 1). For each tunnel velocity 8 separate records of nearly 40 000 images are acquired with total duration of 30 s at $U_\infty = 5.2$ m/s.

The recorded high-speed image data is processed with a coarse-to-fine, iterative cross-correlation algorithm using 3 consecutive frames per time-step. The effective sample size is 64×3 pixel with a wall-normal grid spacing of 1 pixel (Willert et al., 2021). An improved correlation signal is obtained by subtraction of the minimum intensity image followed by intensity capping at 98% of the cumulative intensity range (intensity histogram clipping). From each processed time-step the center column is extracted and compiled into space-time velocity records that are then used for statistics calculations. Mean streamwise velocity profiles and corresponding variances given in Fig. 2 in viscous scaling. Integration of the velocity profiles yields estimates of typical TBL quantities such as the displacement thickness δ^*, momentum thickness θ, shape factor $H = \delta^*/\theta$ and skin friction coefficient c_f. For all flow conditions, the respective values are within 5% bounds of correlations reported in the literature (cf. Fig. 3) and document that the studied flow is representative of a TBL. The characteristic TBL quantities are summarized in Table 2.

Implementation of profile-EBIV

In place of the high-speed camera an event-camera is used. Owing to the high sensitivity and dynamic range (typ. >100 dB) of the event-camera, the lens aperture of the 200 mm macro lens can be stepped down to $f_{\#}8 - f_{\#}16$ while the laser power is also reduced. As described in Willert and Klinner (2022) a low-cost,

Table 1: Measurement parameters for velocity profile measurements on a turbulent boundary layer in air using high-speed PIV and event-based imaging velocimetry.

	HS-PIV			**Profile EBIV**			
Tunnel velocity, U_∞	5.2	7.5	10.0	5.2	7.5	10.0	m/s
Laser pulse rate	10	15	20		10		kHz
Magnification, m		25.0			25.9		μm/pixel
Field of view, $W \times H$		4.0×51.2		5.2×33.1		4.1×33.1	mm²
		160×2048		200×1280		160×1280	pixel
Displacement at U_∞	20.8	20.0	20.0	20.1	29.0	38.6	pixel
Record size		8×38000			(3×100000)		images
Total duration	30.4	20.3	15.2		30.0 [1]		s
Data set size		8×24.0			3×0.90		GB

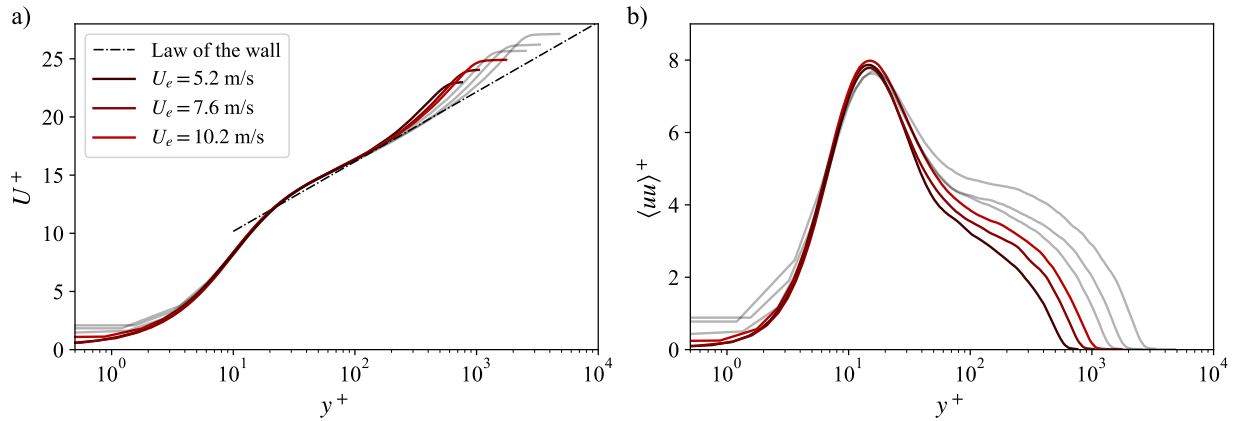[1]) Continuous event records of 60 s duration (5.3 GB) are also available.

Figure 2: Mean velocity profiles (a) and variance of the streamwise velocity component (b) of the studied TBL up to $U_\infty = 30$ m/s obtained with high-speed profile-PIV. Colored profiles are used for comparison with EBIV.
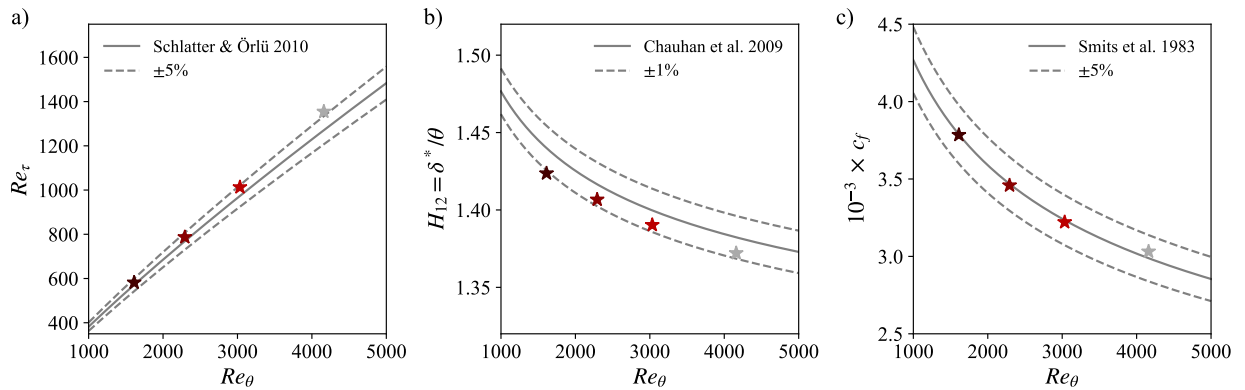

Figure 3: Characteristic quantities of the studied TBL in comparison to correlations reported in the literature. Colored symbols mark data sets acquired with HS profile-PIV and EBIV. Correlations for (a): Schlatter and Örlü (2010), (b): Chauhan et al. (2009) and (c): Smits et al. (1983).

pulse-modulated CW laser is already sufficient to trigger contrast changes of illuminated aerosol tracers. While continuous illumination of the scene is possible, it was found that pulsed illumination improves the time-stamp accuracy of the contrast change events and, at the same time, makes stationary particles visible (Willert, 2023). For the present hardware (EVK2-HD and EVK4-HD, Prophesee S.A.) the events relating to a specific pulse of light can be distinguished for frequencies of up to 10 kHz (period of 100μs). This value is similar to the sensor's readout latency. Reduction of the sensor's region of interest (ROI) also reduces the latency such that light pulses up to 20 kHz are distinctly captured.

2.2   Profile-EBIV measurements of a turbulent boundary layer

Profile-EBIV technique measurements of the TBL described in the previous section are performed at matching flow conditions using the same seeding and laser light sheet as for high-speed PIV. The events generated by laser pulses at 10 kHz are recorded at a rate of $30 \cdot 10^6$ events/s (90 MB/s). For each of three different flow velocities three separate sequences of 10 s duration are recorded. Relevant parameters describing the measurements are given in Table 1.

For off-line processing, the event-stream is first sectioned into pseudo-frame image sequences with a frame period of 100 μs (matching the laser pulsing period). These image sequences can be handled by the same multiple-frame, cross-correlation algorithm used for HS-PIV pocessing. For each time step, 7 pseudo-frames are processed with final sample size of 64×8 pixel. Just as for the profile-PIV measurements, the velocity data is also stored in the form of time-varying velocity profile data sets by retrieving the center column of data from each time-step.

Fig. 4 presents histograms of both velocity components for a complete sequence in comparison to high-speed profile-PIV measurements at the same flow condition. Pixel-locking can be observed in both data sets and is more pronounced for HS-PIV. Although it seems contradictory that the event-data with its drastically reduced bit-depth in comparison to the HS-PIV data seems less prone to pixel locking, it can be reasoned that the use of multiple-frame processing (here $N_f = 7$) leads to an attenuation of the pixel locking effect. The effective size of the event-clusters produced by the imaged particles typically varies between $1.5 - 2.0$ pixel in diameter - and, of course, depends on the lens focus.

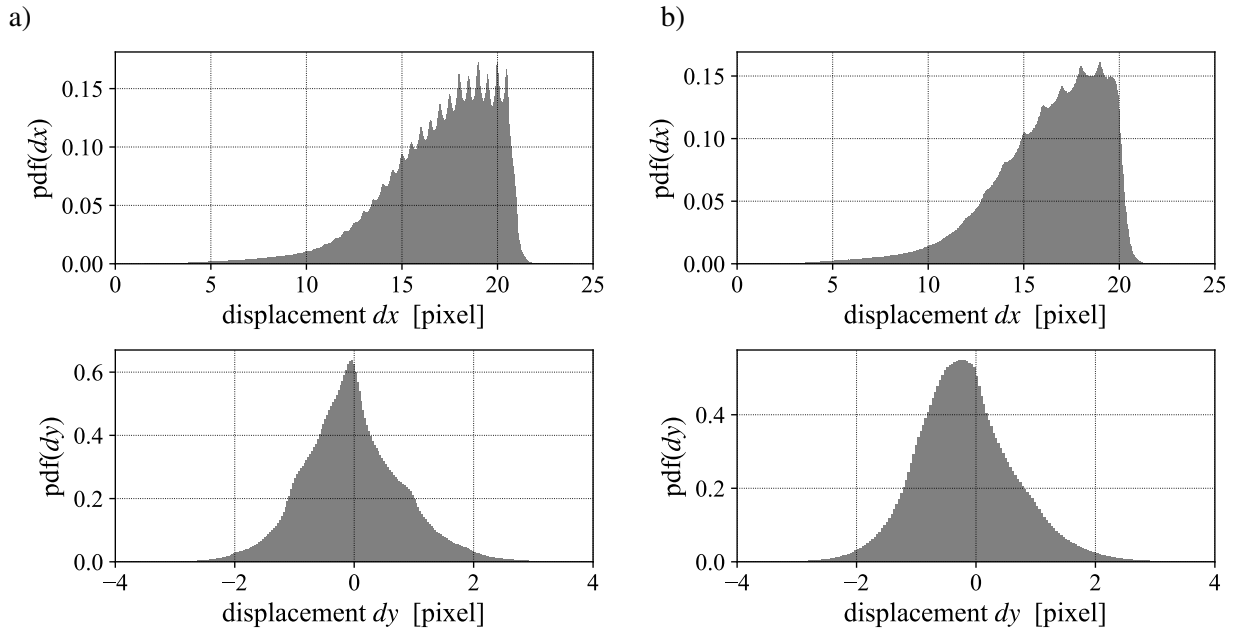a)   b)

Figure 4: Histograms of displacement data obtained with high-speed profile-PIV (a) and profile EBIV (b) from a turbulent boundary layer at $\mathrm{Re}_\tau = 585$. Sample size is $144 \cdot 10^6$ (7.6 s) for HS-PIV and $180 \cdot 10^6$ (10.0 s) for profile EBIV. Bin width is 0.02 pixel.
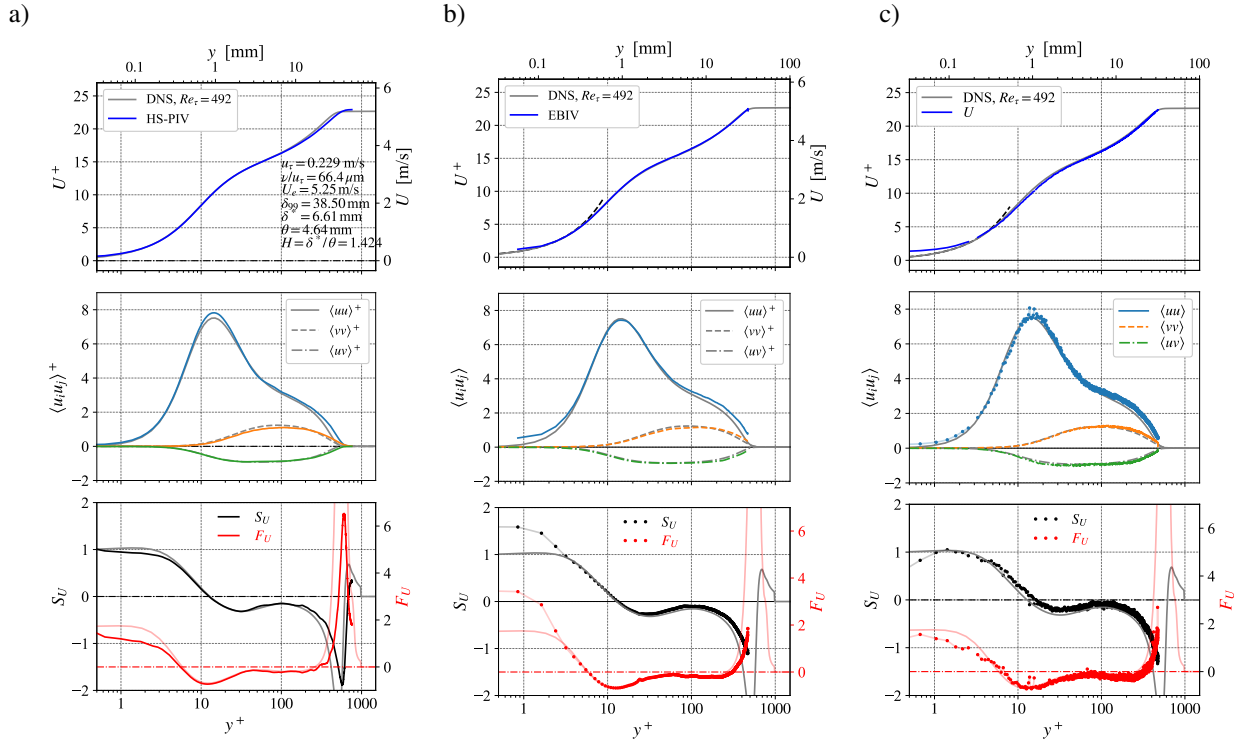
Figure 5: Velocity profiles in viscous scaling obtained with different profile measurement techniques for $Re_\tau = 585$ compared to DNS from Schlatter and Örlü (2010). a: high-speed profile-PIV processed with 64x3 samples; b: event-based imaging processed with 64x8 samples; c: bin-averaged event-based PTV (bin-size 25 μm) Symbols are used in (c) to illustrate the data density.

2.3 Event-based particle tracking

In addition to conventional correlation-based processing of pseudo-images, particle tracking can be also applied to extract the velocity profiles from the event-data. This is accomplished by first extracting event clusters ("blobs") from the event-stream using a temporal sectioning of 100 μs (=10 kHz pulse rate) and computing their spatial centroids (x, y position). The blobs are then tracked along the pseudo-frame sequence. Tracker initialization is either based on the mean field obtained from conventional correlation processing or by an analytical estimate of the mean profile (e.g. Musker, 1979). Efficient particle matching is achieved using the k-d tree space-partitioning data structure. Detected tracks continuously update the predictor field, in this case, the velocity profile. Implemented in C++ the tracker program simultaneously tracks about 2000 particles at a frame rate exceeding 100 Hz such that 10 s of event data are processed within about 10 minutes. This is about 3 orders of magnitude faster than the aforementioned multiple-frame cross-correlation scheme.

3 Results

3.1 Velocity statistics

Mean and higher order statistics are calculated from the time-resolved velocity profile data sets to obtain the data shown in Fig. 5. Here, the both profile-EBIV and tracking results are determined from the same event data set. Overall the results for all measurement schemes are in excellent agreement with DNS data at similar Reynolds number. For the high-speed profile PIV technique an underestimation of the Reynolds stress $\langle uv \rangle$ can be observed at $y^+ < 100$ which is less pronounced for the profile EBIV data. On the other hand profile EBIV exhibits deviations for the streamwise variance $\langle uu \rangle$ as well as higher order moments (skew, kurtosis) in direct proximity of the wall at $y^+ < 3$. While the tracking data generally is more noisy, the variances and higher moments, are in better agreement with the DNS data in comparison to the conventionally (PIV)

Table 2: Characteristic parameters of the studied TBL

Tunnel velocity, U_∞	5.2	7.5	10.0	m/s
Edge velocity, U_e	5.25	7.57	10.17	m/s
BL thickness, δ_{99}	38.7	38.1	36.8	mm
Displacement thickness, δ^*	6.61	6.47	6.19	mm
Momentum thickness, θ	4.64	4 .60	4.45	mm
Shape factor, $H = \delta^*/\theta$	1.425	1.407	1.391	
Friction velocity, u_τ	0.228	0.314	0.408	m/s
Viscous unit, ν/u_τ	66.2	48.1	37.0	μm
Friction Reynolds number, Re_τ	585	793	995	
Reynolds number, Re_θ	1610	2310	3000	
Reynolds number, $Re_{\delta_{99}}$	13500	19100	24800	

processed data. This is attributed to the fact a PTV is not directly affected by spatial sampling artifacts characteristic of correlation-based schemes. The overestimation of the mean flow close to the wall at $y^+ < 2$ by event-based particle tracking velocimetry (EB-PTV) could be caused by a reduced sensitivity of the EBV camera to slowly moving particles: depending on the camera's refractory period (i.e. pixel reset time), a given pixel may not trigger a new event for the immediately following light pulse. for this situation, the tracker algorithm currently is not able to initiate a new track.

3.2 Space-time correlations and spectra

The time-resolved nature of the velocity profile data allows the calculation of spatially resolved correlations and spectra. In the following, space-time velocity records with $U_\infty = 5.2\,\text{m/s}$ and total duration of $30\,\text{s}$ acquired at $10\,\text{kHz}$ laser pulsing rate are used.

The autocorrelations of both measured velocity components spatially resolved in the wall-normal distance y are provided in Fig. 6. Overall, the correlation maps are in good agreement for both velocity components, even at lower correlation levels $R_{uu} < 0.2$ that are more susceptible to noise. Differences are present at a wall-distance of $y/\delta_{99} > 0.5$ where the EBIV data exhibits a minimum for $R_{uu} < 0.2$ and begins to increase again. This area is also characterized with spikes that are believed to result from periodically firing *hot* pixels of the EBV sensor.

While similar autocorrelation maps in principle can be obtained with single-point measurement techniques, this effort becomes challenging for two-point correlations where a velocity record at a given wall-distance y_0 is compared to all other points along the y-axis. Exemplary two-point correlation maps are presented in Fig. 7 for two wall distances: at the peak of streamwise turbulence ($y_0 = 13.5^+$) and within the logarithmic layer ($y_0 = 100^+$). Again, the quantitative differences between profile-PIV and profile-EBIV are minimal for correlation values $R_{uu} \geq 0.2$. At lower values $R_{uu} \leq 0.1$ profile-EBIV predicts larger correlation domains, in particular for the streamwise valocity component u. In part, this may also be associated with the stripe artifacts observed in the autocorrelation maps at $y/\delta_{99} > 0.5$.

Fig. 8 shows spatially resolved, pre-mulitplied power spectra calculated from the data sets provided by both measurement techniques. The low-pass filter cut-off is set at $f_{lp} = f_{acq}/3 = 3.33\,\text{kHz}$. The spectra are pre-multiplied with the frequency axis in order to highlight their respective spatial distribution. While the spectra exhibit both visual as well as quantitative agreement, there are discrepancies at the upper frequencies ($f \gtrsim 1\,\text{kHz}$) and in proximity to the wall ($y^+ < 3$) as already noted for the EBIV velocity profile data. It should be observed that the spectra are computed from the time-resolved velocity profiles without additional validation, that is, they include effects from possible outlier data. Just as for the correlation maps, at $y/\delta_{99} > 0.5$ the streamwise EBIV velocity component exhibits artifacts in the form of horizontal lines in the power spectrum. Differences in the relative positions of the energy maxima are caused by the relatively flat plateaus that are susceptible underlying noise. Regardless, the shape of the contours are in good agreement for reduced energy levels of $f^+ \phi_{u,u}/u_\tau^2 \geq 0.01$, which further underlines the potential of time-resolved velocity profile measurement using event-based imaging.
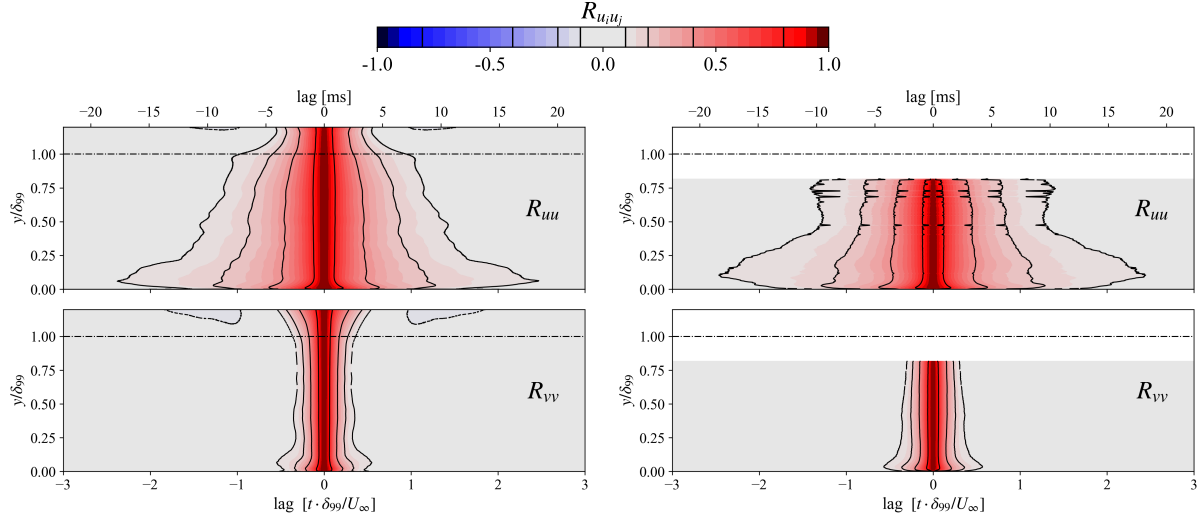
Figure 6: Autocorrelation maps of both velocity components for high-speed profile-PIV (left column) and profile-EBIV (right column) at $Re_\tau = 585$. Top: streamwise velocity component u; bottom: streamwise velocity component v. Black contour lines are at $\pm0.1, \pm0.2, \pm0.4, \pm0.8$.

4 Summarizing remarks and conclusions

The presented material provides clear evidence that the data obtained with EBIV is of similar quality as conventional PIV. The currently available EBV camera hardware used in the present implementation is limited to maximum effective framing rates (i.e. laser pulsing rates) of 10 kHz which is directly coupled to the event camera's latency ($\approx 100\,\mu s$). This frequency limit may be raised with the availability of newer hardware generations. While not presented herein for reasons of brevity, EBIV data of similar quality was obtained at up to $U_\infty = 10$ m/s at the same image magnification. At even higher velocities the particle image displacements become too large to be adequately handled by the PIV and PTV processing schemes. For this purpose, EBV camera hardware with a latency considerably lower than $100\,\mu s$ are required.

Processing the pseudo-frames derived from the event-data with iterative correlation-based schemes is rather slow, precluding a possible real-time implementation such as for the *TrackAER* system introduced by Rusch and Rösgen (2022). The data presented in the previous sections required on the order of 3-4 hours to process 100 000 pseudo-frames (10 s of event data) on an 8-core workstation. While not yet fully optimized, the event-based particle tracking algorithm processed the same data within 10 min at a rate of 200 pseudo-frames per second on a single processor core.

A clear advantage of the event-based imaging velocity profile measurement technique is its significantly reduced storage demand. As illustrated in the preceding sections with an exemplary measurement of a TBL, the raw data of a corresponding PIV measurement requires roughly 45 times more space (cf. Table 1, accounting for image size). However, this comes at the price of reduced image bit-depth (1 bit/pixel) with its implications on the measurement uncertainty and increased noise. On the other hand, the reduced data stream allows the recording of considerably longer data sets than are feasible with currently available high-speed cameras. Within this work records of up to 60 s were acquired at about 100 MB/s (6 GB total). From a cost perspective the "savings" amounts to a factor of 20-40 on the camera side assuming a frame rate capability of 10 kHz at 1280×200 pixel. Beyond this, the high light sensitivity of the event camera technology in comparison to conventional (CMOS) sensors permits the use of lasers with significantly reduced pulse energies ($25 - 50\,\mu J$ per pulse). For similar EBIV measurements in air Willert (2023) used a low-cost (≈ 250 Euro) engraving laser.

References

Borer D, Delbruck T, and Rösgen T (2017). Three-dimensional particle tracking velocimetry using dynamic vision sensors. *Experiments in Fluids* 58(165). doi:10.1007/s00348-017-2452-5. URL https://doi.
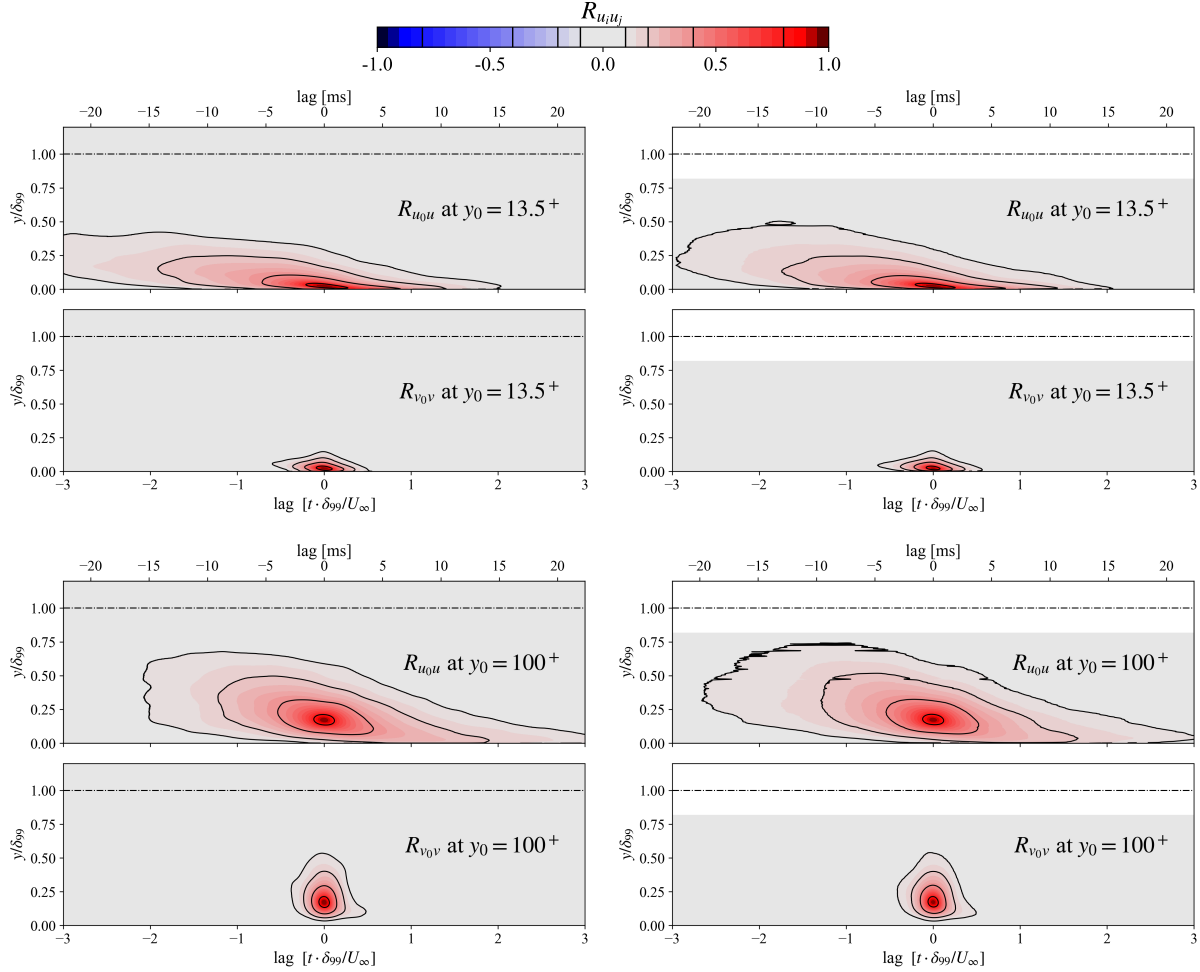
Figure 7: Two-point correlation maps of both velocity components at two wall-distances for high-speed profile-PIV (left column) and profile-EBIV (right column) at $\mathrm{Re}_\tau = 585$. Top: streamwise velocity component u; bottom: streamwise velocity component v. Black contour lines are at $\pm 0.1, \pm 0.2, \pm 0.4, \pm 0.8$.

org/10.1007/s00348-017-2452-5

Chauhan K A, Monkewitz P A, and Nagib H M (2009). Criteria for assessing experiments in zero pressure gradient boundary layers. *Fluid Dynamics Research* 41(2):021404. ISSN 0169-5983, 1873-7005. doi: 10.1088/0169-5983/41/2/021404

Cuvier C, Srinath S, Stanislas M, Foucaut J M, Laval J P, Kähler C J, Hain R, Scharnowski S, Schröder A, Geisler R, Agocs J, Röse A, Willert C, Klinner J, Amili O, Atkinson C, and Soria J (2017). Extensive characterisation of a high Reynolds number decelerating boundary layer using advanced optical metrology. *Journal of Turbulence* 18(10):929–972. doi:10.1080/14685248.2017.1342827. URL http://dx.doi.org/10.1080/14685248.2017.1342827

Drazen D, Lichtsteiner P, Haefliger P, Delbruck T, and Jensen A (2011). Toward real-time particle tracking using an event-based dynamic vision sensor. *Experiments in Fluids* 51(1):1465–1469. doi:10.1007/s00348-011-1207-y. URL http://www.zora.uzh.ch/60624/1/Drazen_EIF_2011.pdf

Gallego G, Delbrück T, Orchard G, Bartolozzi C, Taba B, Censi A, Leutenegger S, Davison A J, Conradt J, Daniilidis K, and Scaramuzza D (2022). Event-based vision: A survey. *IEEE Transactions on Pattern Analysis and Machine Intelligence* 44(1):154–180. doi:10.1109/TPAMI.2020.3008413. URL https://arxiv.org/pdf/1904.08405.pdf

Howell J, Hammarton T C, Altmann Y, and Jimenez M (2020). High-speed particle detection and tracking in microfluidic devices using event-based sensing. *Lab Chip* 20:3024–3035. doi:10.1039/D0LC00556H. URL `http://dx.doi.org/10.1039/D0LC00556H`

Musker A J (1979). Explicit expression for the smooth wall velocity distribution in a turbulent boundary layer. *AIAA Journal* 17(6):655–657. ISSN 0001-1452, 1533-385X. doi:10.2514/3.61193. URL `https://arc.aiaa.org/doi/10.2514/3.61193`

Rusch A and Rösgen T (2021). TrackAER: Real-time event-based particle tracking. In *14th International Symposium on Particle Image Velocimetry (ISPIV 2021)*, p. 176. Illinois Institute of Technology, Chicago, IL. doi:10.18409/ispiv.v1i1.176

Rusch A and Rösgen T (2022). Online event-based insights into unsteady flows with TrackAER. In *20th International Symposium on Application of Laser and Imaging Techniques to Fluid Mechanics*. Lisbon, Portugal

Schlatter P and Örlü R (2010). Assessment of direct numerical simulation data of turbulent boundary layers. *Journal of Fluid Mechanics* 659:116–126. ISSN 0022-1120, 1469-7645. doi: 10.1017/S0022112010003113. URL `https://www.cambridge.org/core/product/identifier/S0022112010003113/type/journal_article`

Smits A J, Matheson N, and Joubert P N (1983). Low-Reynolds-number turbulent boundary layers in zero and favorable pressure gradients. *Journal of Ship Research* 27(03):147–157. ISSN 0022-4502. doi: 10.5957/jsr.1983.27.3.147. URL `https://doi.org/10.5957/jsr.1983.27.3.147`

Willert C (2015). High-speed particle image velocimetry for the efficient measurement of turbulence statistics. *Experiments in Fluids* 56(1):17. ISSN 0723-4864. doi:10.1007/s00348-014-1892-4. URL `http://dx.doi.org/10.1007/s00348-014-1892-4`

Willert C (2023). Event-based imaging velocimetry using pulsed illumination. *Experiments in Fluids* 64:98. doi:10.1007/s00348-023-03641-8. URL `https://doi.org/10.1007/s00348-023-03641-8`

Willert C, Cuvier C, Foucaut J, Klinner J, Stanislas M, Laval J, Srinath S, Soria J, Amili O, Atkinson C, Kähler C, Scharnowski S, Hain R, Schröder A, Geisler R, Agocs J, and Röse A (2018). Experimental evidence of near-wall reverse flow events in a zero pressure gradient turbulent boundary layer. *Experimental Thermal and Fluid Science* 91(Supplement C):320 – 328. ISSN 0894-1777. doi:10.1016/j.expthermflusci. 2017.10.033. URL `http://www.sciencedirect.com/science/article/pii/S0894177717303394`

Willert C and Klinner J (2022). Event-based imaging velocimetry: An assessment of event-based cameras for the measurement of fluid flows. *Experiments in Fluids* 63:101. doi:10.1007/s00348-022-03441-6. URL `https://doi.org/10.1007/s00348-022-03441-6`

Willert C, Schanz D, Novara M, Geisler R, Schroll M, Ribergard S, and Schröder A (2021). Multi-resolution, time-resolved piv measurements of a decelerating turbulent boundary layer near separation. In *14th International Symposium on Particle Image Velocimetry (ISPIV 2021)*. doi:10.18409/ispiv.v1i1.77. URL `https://doi.org/10.18409/ispiv.v1i1.77`

Willert C, Soria J, Stanislas M, Klinner J, Amili O, Eisfelder M, Cuvier C, Bellani G, Fiorini T, and Talamelli A (2017). Near-wall statistics of a turbulent pipe flow at shear Reynolds numbers up to 40 000. *Journal of Fluid Mechanics* 826. doi:10.1017/jfm.2017.498. URL `http://dx.doi.org/10.1017/jfm.2017.498`
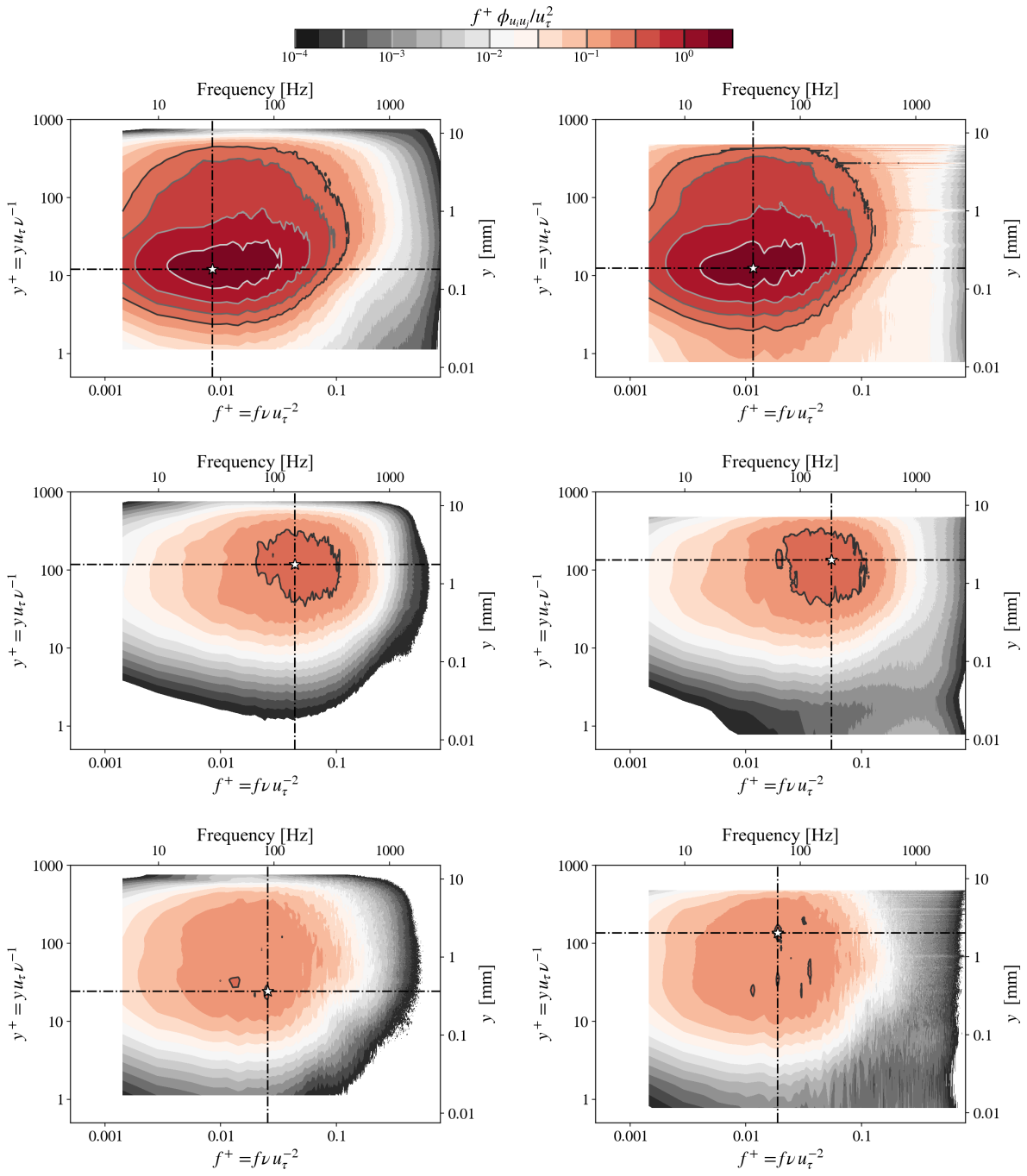
Figure 8: Inner-scaled, premultiplied power spectra for high-speed profile-PIV (left column) and profile-EBIV (right column) at $\mathrm{Re}_\tau = 585$. Top row: streamwise velocity component u; middle row: streamwise velocity component v; bottom row: Reynolds stress $\langle uv \rangle$.